16B.5 Evaluation of the MYNN PBL Scheme Closure Constants for Low-Level Jet Events in a Stable Boundary Layer

DAVID E. JAHN, * WILLIAM GALLUS, AND EUGENE S. TAKLE

Dept. of Geological and Atmospheric Sciences, Iowa State University, Ames, IA

1 Introduction

Accurate forecasts of wind at turbine height are crucial for the integration of wind as a viable and dependable energy source. Wind, however, is inherently variable and poses a challenge to utility operators. Although operators have in place certain means of dealing with some wind power variability, such as maintaining an appropriate level of reserve generation as needed, large and unexpected fluctuations in wind speed over a relatively short period of time can have significant impact on utility operations and can be very costly.

A significant drop in wind power, for example, would require the use of a large portion of reserve generation, which in turn may present the need to bring on-line conventional generation in a relatively short time. Such a scenario could be costly depending on start-up and operation costs. In the case of an unexpected large increase in wind power, wind generation may need to be curtailed to maintain load balance, which is a waste of resources, or, if the wind increase is such to exceed the operating parameters of the deployed wind turbines, an entire wind farm may need to be shut down for a period, causing a potentially severe shortage in power generation. Such large changes in wind speed over a relatively short time period are referred to as wind ramps.

There is no one uniformly accepted definition as to what constitutes a wind ramp. Certain studies have used the criteria of a 50% change in wind generation as compared to total power capacity within a period of 4 hours or less Greaves et al. (2009); Deppe et al. (2013) and others have used the criteria of 20% power change over either a 30-minute period or less (Freedman et al., 2008) or 1 hour or less (Bradford et al., 2010). An increase in power equal to 50% of a power capacity of 1500 kW, for example, would occur with an increase in wind by 3 m/s as is consistent with the power curve of a 1.5-MW wind turbine as shown in Fig. 1 and referenced in Deppe et al. (2013). The criteria for a wind ramp selected in this study is the increase or decrease of wind velocity by at least 3 m/s over a 1-hour period or less.

There is much room for improvement for wind ramp forecasts, or for wind forecasts at turbine-height in general. For example, 6-hour forecasts of low-level winds over North America produced by the Rapid Refresh (RAP) model, which is used operationally by the National Weather Service (NWS), are defined by a 3-4 m/s RMS er-

* *Corresponding author address:* Dept. of Geological and Atmospheric Sciences, Iowa State University
E-mail: djahn@iastate.edu

ror as compared against rawinsonde upper-air observations (Benjamin et al., 2013). For a site with average turbine-height wind speed of 10 m/s, this error represents, in general, a value more than 30% of the observed wind.

Such statistics are similar to those published in a report published by the Mid-continent Independent System Operator (MISO, Navid et al. (2011)), which indicated a wind generation day-ahead forecast error of 8-10% of wind generation capacity, representing up to 30% of actual wind generation. A 15-month study by Greaves et al. (2009) found that commercially provided day-ahead forecasts had an accuracy of 30% for select US sites and 35% for UK sites in the prediction of wind ramp events.

For a study of a wind farm site in Iowa, Deppe et al. (2013) simulated a suite of ramp events using a numerical forecast model with a variation of boundary layer schemes. Like Greaves et al. (2009), they also found that the number of ramp events were under forecast. The highest forecast accuracy rating they achieved for a day-ahead forecast horizon of ramp up events using their suite of model configurations was just over 40%.

In order to improve wind forecasts, there is general consensus that much work needs to be done to improve, in particular, the PBL schemes used by numerical weather prediction (NWP) models. Such consensus is evidenced by a Department of Energy workshop report on wind resource characterization (S. Schreck, 2008) and by individual studies. For example, Storm and Basu (2010) investigated wind events in KS and TX and found that the height of the low-level jet (LLJ) was overestimated and wind speed underestimated in their simulations using two different PBL schemes, a result that they suggested was due to artificially enhanced mixing. As mentioned above, Deppe et al. (2013) found differences in model performance depending on the PBL scheme invoked, and concluded overall that there was not demonstrated an acceptable prediction capability for ramp events.

Such studies are useful in defining a performance record for existing PBL schemes, but it would be all the more beneficial to critically assess through quantitative analysis what are the technical reasons why a given PBL scheme falls short in forecasting ramp events and for turbine-height winds in general. Such effort would require an investigation of the fundamental theory of a given scheme, such as how a scheme represents the (complex) dynamics of the atmospheric boundary layer.

There have been very few studies to date, which have sought to modify a PBL scheme itself beyond the introduction of a scheme by its original authors. The exception is the work described in Olson and Brown (2012), which modified the means by which turbulent eddy scale factors (e.g. turbulent mixing lengths) are diagnosed in a given PBL scheme. Their work is of value and has realized considerable improvement for upper-level winds in NWS operational wind forecasts as well as some improvement to near-surface winds forecasts (Olson and Brown, 2011, 2012). Their focus in improving a PBL scheme, however, is broad in seeking scheme modifications that perform well across all weather regimes and scenarios, which is very difficult.

The fact is that the role and prominence of specific dynamics can vary depending on the weather phenomenon and the formulation of a PBL scheme to correctly represent these dynamics would also vary by phenomenon. This is true even if just considering wind ramp events, the causes of which can be very different. It is difficult to formulate a "one size fits all" scheme for all ramp events let alone all weather phenomena, which has been the trend to date in the NWP community. Within the modeling community, there is a call (even

an "urgent" call by some) for a specific focus on improving the PBL scheme especially as related to the nocturnal stable boundary layer (SBL), primarily because of the excessive mixing of the boundary layer by the model as well as pronounced cooling at the surface (Grisogono, 2010; Fernando and Weil, 2010; Hu et al., 2013). Both effects can dramatically impact the evolution of the boundary layer and thus wind forecasts.

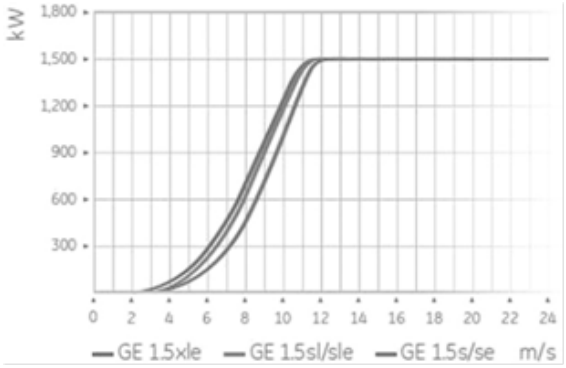

Figure 1: Example power curve for 1.5MW GE wind turbine as presented in Deppe et al. (2013).

The purpose of this current study is to revisit the formulation of the MYNN scheme (described in a subsequent section), looking specifically at the closure constants, which are used to define an approximated linear interdependence of covariance turbulence variables, such as momentum and heat fluxes. These approximations serve as the means of closing the system of 2nd-order turbulence equations. The MYNN scheme is available as a PBL scheme in the WRF code and is a widely used option for both operational runs by the NWS (Benjamin et al., 2013) and within the research community. Because the causes and thus forecast issues can vary for different wind ramp events, it was selected to narrow the focus in this study to idealized simulations based on events occurring in the presence of a nocturnal stable boundary layer (SBL).

2 Background

PBL schemes represent the subgrid processes that emulate the effects of surface drag and cooling/heating in the overlying flow and determine the degree of stability of the lowest portion of the atmosphere. An example is the cooling of the surface over night due to the emission of longwave radiation, by which the air just above the surface cools relative to overlying air thus creating a stably stratified layer.

The mixing of the atmosphere, such as through turbulent eddies, would tend to counter the set up of a strong vertical gradient and reduce the stability strength. The PBL schemes thus serve an effectual role in determining the generation or dispersion and diffusion of turbulence and the degree to which a stable stratification is maintained.

The underlying theory of the MYNN scheme is based on the fundamental equations of conservation of mass, momentum. The presentation below follows closely that given by Mellor (1973), Mellor and Yamada (1974), and Mellor and Yamada (1982) (heretofore referred to as M73, MY74, and MY82 respectively). The continuity equation, equation of motion for mean velocity, U_j, and conservation of mean potential temperature, Θ, are

$$\frac{\partial U_k}{\partial x_k} = 0 \tag{1}$$

$$\frac{\partial U_j}{\partial t} + \frac{\partial}{\partial x_k}(U_k U_j + \overline{u_k u_j}) + \epsilon_{jkl} f_k U_l = -\frac{1}{\rho}\frac{\partial P}{\partial x_j} - g\delta_{j3}\beta\Theta + \nu\nabla^2 u_j \tag{2}$$

$$\frac{\partial \Theta}{\partial t} + \frac{\partial}{\partial x_k}(U_k\Theta + \overline{u_k\theta}) = \alpha\nabla^2\Theta \tag{3}$$

for which Einstein summation notation has been adopted. Here P is mean pressure, while u_j, θ, and p are fluctuations about the

mean values of wind velocity, potential temperature, and pressure respectively. Expressions with an overbar represent Reynolds averaged values. Also, g represents the (vertical) gravity vector, f is the Coriolis parameter, and β the coefficient of thermal expansion ($\beta = -(\partial\rho/\partial T)/\rho$) while ν represents kinematic viscosity and α kinematic heat conductivity.

In order to obtain a closed solution for these set of equations, it is necessary to obtain values for the moment and heat flux variance terms $\overline{u_i u_j}$ and $\overline{u_i\theta}$, which altogether represent 9 combinations of variables. The governing equations for these variables are detailed in M73, MY74, and MY82 as well as Nakanishi (2001) (herein denoted as N01) and given here:

$$\frac{\partial\overline{u_i u_j}}{\partial t} + \frac{\partial(U_k\overline{u_i u_j})}{\partial x_k} + \overline{u_k u_i}\frac{\partial U_j}{\partial x_k} + \overline{u_k u_j}\frac{\partial U_i}{\partial x_k} = E_{distr} + E_{disp} + B + F \quad (4)$$

where E_{distr} is the energy distribution term, E_{disp} is energy dissipation, B buoyancy, and F is the Coriolis term.

$$\frac{\partial\overline{u_j\theta}}{\partial t} + \frac{\partial(U_k\overline{\theta u_j})}{\partial x_k} + \overline{u_j u_k}\frac{\partial\Theta}{\partial x_k} + \overline{\theta u_k}\frac{\partial U_j}{\partial x_k} = T_{distr} + T_{disp} + B \quad (5)$$

Such that T_{distr} and T_{disp} denote energy distribution, dissipation, and diffusion terms.

This system requires solving 9 differential equations. For practical purposes, certain simplifications are warranted. The approach used in the MYNN scheme was based on a series of assumptions and simplifications as are detailed in M73, MY74, MY82 and N01, and which include the boundary-layer approximation and neglecting time-tendency, advection, and diffusion terms. The resulting simplified set of equations (denoted as a Level 2 model by the noted authors) are presented in N01 as

$$\overline{u^2} = \gamma_1 q^2 + 2A_1C_2\frac{L}{q}\frac{g}{\Theta_o}\overline{w\theta} - 6A_1\frac{L}{q}\overline{uw}\frac{\partial U}{\partial z} \quad (6)$$

$$\overline{v^2} = \gamma_1 q^2 + 2A_1C_2\frac{L}{q}\frac{g}{\Theta_o}\overline{w\theta} \quad (7)$$

$$\overline{w^2} = \gamma_1 q^2 + 2A_1(3-2C_2)\frac{L}{q}\frac{g}{\Theta_o}\overline{w\theta} \quad (8)$$

$$\overline{uw} = 3A_1\frac{L}{q}[-(\overline{w^2}-C_1q^2)\frac{\partial U}{\partial z} + (1-C_2)\frac{g}{\Theta_o}\overline{u\theta}] \quad (9)$$

$$\overline{u\theta} = 3A_2\frac{L}{q}[-\overline{uw}\frac{\partial\Theta}{\partial z} - (1-C_5)\overline{w\theta}\frac{\partial U}{\partial z}] \quad (10)$$

$$\overline{w\theta} = 3A_2\frac{L}{q}[-\overline{w^2}\frac{\partial\Theta}{\partial z} + (1-C_3)\frac{g}{\theta_o}\overline{\theta^2}] \quad (11)$$

$$q^2 = B_1\frac{L}{q}(-\overline{uw}\frac{\partial U}{\partial z} + \frac{g}{\theta}) \quad (12)$$

$$\overline{\theta^2} = -B_2\frac{L}{q}\overline{w\theta}\frac{\partial\Theta}{\partial z}. \quad (13)$$

Note that although the MYNN scheme itself is based on Level-2.5 and Level-3.0 equations, these simplified Level 2.0 equations are used to derive the closure constants in N01, the method of which is the focus of this paper.

The variables in these equations remain as earlier defined, although the coordinate system has been oriented such that $\overline{vw} = 0$. The equation for q^2 represents twice the TKE ($q^2 = u^2 + v^2 + w^2$). L represents a turbulent master length scale associated with anticipated eddy size. Note that the above equations include a set of closure constants ($A_1, A_2, B_1, B_2, C_1, C_2, C_3, C_5$) , which are the result of certain approximations that define a linear dependence of turbulent covariance variables on gradients of other covariance variables or variables of the mean flow. Also $\gamma_1 = 1/3 - 2A_1/B_1$.

Of interest to this specific study is the dissipation term. In the works of M73 and MY74 energy dissipation in Eq. 4 is directly related

to the downscaling of turbulent kinetic energy, q^2:

$$-2\nu\overline{\frac{\partial u_i}{\partial x_k}\frac{\partial u_j}{\partial x_k}} = -\frac{2}{3}\frac{q^3}{B_1 L}\delta_{ij} \qquad (14)$$

where ν is kinematic viscosity.. An analogous thermodynamic relation was also used for the dissipation term of Eq. 5:

$$-2\alpha\frac{\partial\theta}{\partial x_k}\frac{\partial\theta}{\partial x_k} = -2\frac{q}{B_2 L}\bar{\theta^2}, \qquad (15)$$

where α is thermal diffusivity.

The work presented in N01 was to define appropriate values for each of these closure constants. A set of LES simulations was initiated with the same neutral thermodynamic structure, but with different constant heat fluxes at the surface, both positive and negative, as to promote thermal stratification of various degrees of stability/instability near the surface. The resulting data were used to calculate explicitly covariance variables such as in the equations above and thus, consistent with the dynamic relationships among the variables as defined in the above equations, identify specific values for the closure constants that are appropriate for all test cases.

It is interesting to note, though, that in order to identify values for the closure constants, N01 simplified yet further the set of equations above by invoking similarity theory. Such approximations may be appropriate for the surface layer but may not necessarily be applicable for higher levels of the BL and particularly for LLJ cases for which the vertical wind profile does not follow standard log-law characterization.

In consideration of a need to improve wind forecasts by improving the depiction and evolution of BL winds in mesoscale models, the purpose of this study is to initiate an effort to re-evaluate the closure terms of the MYNN scheme specifically in context of LLJ cases in the SBL and in consideration of levels above the surface layer.

3 Methodology

The first step is to identify the sensitivities that mesoscale numerical wind forecasts have to small or large variations in the closure constants, $B1$ and $B2$, which are associated with energy dissipation. Forecasts are generated using a mesoscale model for three weather events that exhibit a wind ramp associated with the set up of a low-level jet within a nocturnal SBL.

The second step of this study is to formulate values for the closure constants as appropriate for LLJ cases in a SBL. For such wind ramp cases, turbulence-scale data are generated by a LES model, by which explicitly-derived turbulence variance data are used to calculate values for $B1$ and $B2$. The models and methodologies used in this study are described below.

3.1 Identifying mesoscale wind forecast sensitivity to closure constants

Wind and temperature observations from a 200m tower near Mason City, IA were used to identify three events for this study. Chosen cases exhibited a wind ramp associated with the set-up of a nocturnal LLJ in a SBL and with evidence of no other larger-scale forcings such as from a frontal passage or nearby storms.

The tall tower data, which represent a continuous record of 10-minute averaged observations at 50m, 100m, 150m, and often 200m heights [AGL], were provided through the Iowa Energy Center, which supported a project to instrument several tall towers in Iowa and collect meteorological data for a little over two years starting in late 2006.

The numerical model used in this study to generate a suite of mesoscale numerical wind forecasts for select ramp event cases

was the Weather Research and Forecasting (WRF) model, version 3.5.1. The NWS North American Regional Re-analysis (NARR) data files were used for model boundary and initial conditions. All forecasts were initialized at 18 UTC on the first day of the respective case and ended at 12 UTC the following day (an 18-hour forecast horizon).

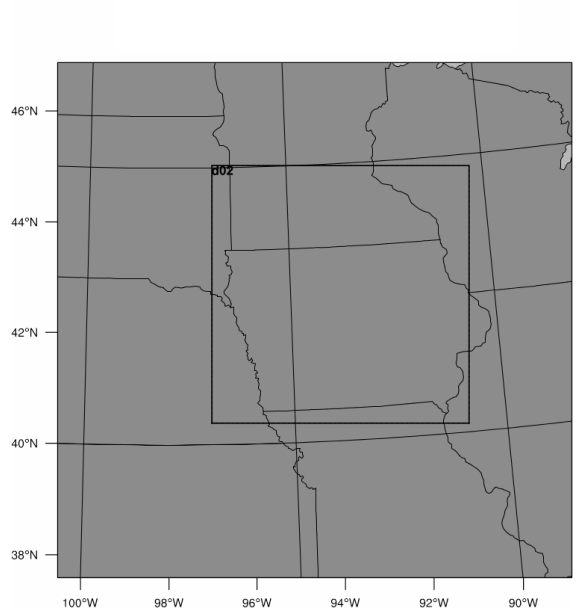

Figure 2: Nested domains used for WRF simulations.

Two one-way nested grids were used as shown in Fig. 2 and consisted of horizontal resolutions of 10-km and 3.33-km respectively. Vertically, the domains were depicted by a stretched grid of 46 sigma levels up to 100mb. At and below 250m, the specific levels in the model included 7.8m, 21.6m, 37.2m, 52.9m, 68.6m, 84.36m, 104.1m, 133.7m, 177.2m, and 250.8m [AGL]. As mentioned above, the PBL scheme used for all tests was the MYNN scheme along with Noah Land-Surface scheme (F. Chen, 2001). The WRF Single-Moment 5-Class (WSM5) microphysics scheme (Hong et al., 2004) was used for all runs, and the cumulus parameterization scheme of Kain-Fritsch (Kain, 2004) was used only for the 10-km grid. Shortwave radiation processes were represented by the Dudhia scheme (Dudhia, 1989) and longwave radiation by the rapid radiative transfer model (RRTM) (E.J. Mlawer, 1997).

In order to evaluate wind forecast sensitivity to closure constants, the WRF model is re-run for each case using values of $B1$ or $B2$ that are half and then also twice the values used for a control run ($B1 = 24.0$ and $B2 = 15.0$) as are hard-coded in the MYNN scheme. The basis for varying these closure constants in such a way is influenced by the various values that have been proposed in the literature for both the MYJ and MYNN schemes (M73, MY74, N01, and Nakanishi and Niino (2004)). It should be noted that all other closure constants, such as those associated with the energy distribution term, are kept at their initial MYNN values. The modeled wind forecasts resulting from this suite of sensitivity tests are analyzed by calculating a percentage change in wind velocities that exist relative to the forecast velocities of the control run.

3.2 Calculating closure constants using LES-derived turbulence data

A LES version of the WRF model is run using a finely-resolved computational grid such that turbulent eddies of extent 20m and larger are explicitly resolved. The LES version used in this study is described in Yamaguchi and Feingold (2012) and is based on WRF version 3.3.1. A grid spacing of 4m is used horizontally for a computational domain consisting of 96x96 points. This domain is identical to the domain of N01. The vertical grid consists of 239 points with a constant resolution of 4m for the first 200 points (750m AGL) and a stretched grid to the top (1296m AGL).

The cases chosen for this study consist

of an environment that is horizontally homogeneous and thus it is plausible to initialize the model with a single vertical sounding of temperature and wind data. Large-scale forcings outside the domain are not considered and thus horizontal periodic boundary conditions are invoked. However, a specific constant cooling flux is maintained at the surface. Precipitation effects are not included and thus all moist processes are turned off. Subgrid processes are parameterized using a 1.5 order TKE closure scheme that is based on a prognostic equation for TKE and a mixing coefficient based on TKE and an empirically-defined mixing length. These LES simulations are executed using a Linux system consisting of 17 nodes (2 Intel Xeon processors per node) as part of the computing platform within the Department of Geological and Atmospheric Science at Iowa State University.

Although the LES simulations are idealized, their initial states are based on real cases as analyzed using the mesoscale model described above. The single sounding that depicts the base state for the LES simulation is extracted from the center of the domain of a 3-km model simulation of a selected LLJ case. The LES model is initiated at a time after the development of the jet and run over a 2-hour period for which the mean state (the resolved state of the mesoscale model) is relatively steady as evidenced by a vertically integrated TKE that is quasi-stationary.

Although the MYNN scheme contains 8 empirically-defined closure constants that warrant investigation, only two closure constants, B_1 and B_2, are evaluated herein simply as a means to limit the scope of the present study. These two constants were chosen because they exist as the only closure constant in their respective variance equations and thus their appropriate values are more easily derived.

The approach to formulate values for the closure constants follows that as outlined in N01, although specifically for experiments involving a LLJ in a stable boundary layer. Similar to N01, experimental data of relatively fine-scale resolution will be generated using a LES model, as described above. These data can be used to represent explicitly the perturbation values for wind and temperature: u, v, w and θ. Reynolds-averaged covariances can then be calculated along with the mean wind in order to evaluate Eqs. 12 and 13. Specifically, the objective is to identify whether a single value for each closure constant can be identified such that the dynamic relationships as posed by the equations are indeed valid especially in the context of the LLJ cases of this study.

One value of B_1 needs to be set such that there is maintained a TKE production-dissipation balance according to Eq. 12. Using the LES data and invoking Reynolds averaging, it is possible to explicitly represent the momentum and heat fluxes that comprise these terms in order to investigate the veracity of Eq. 12 over the entire domain for a given case. The mean wind and potential temperature are also known such that it is possible to identify one value of B_1 for a given case at one select time and vertical level (through Reynolds averaging the solution is horizontally homogeneous). The crux of this study is to investigate whether Eq. 12 using one defined value of B_1 remains valid across the various cases and for different vertical levels in the BL.

A similar procedure is undertaken to investigate Eq. B_2, although based on an evaluation of 13 using the LES data for the given cases.

4 Results

4.1 Mesoscale Wind Forecast Sensitivity to Closure Constants

The WRF model was used to generate mesoscale wind forecasts for three arbitrary LLJ cases occurring near Mason City, IA during 2007-08, and for which the closure constants, $B1$ and $B2$ were systematically varied in magnitude. The remaining closure constants, C_n and A_n, remained set to original values as prescribed in the MYNN scheme. For each test case, four WRF simulations were run such that $B1$ and $B2$ were individually set to twice and then half their original values ($B1 = 24.0$ and $B2 = 15.0$) as used for the control run. $B2$ was kept at its original value when $B1$ was varied and *vice versa*. The percentage changes in forecasted winds resulting from varying closure constant values are given in Table 1.

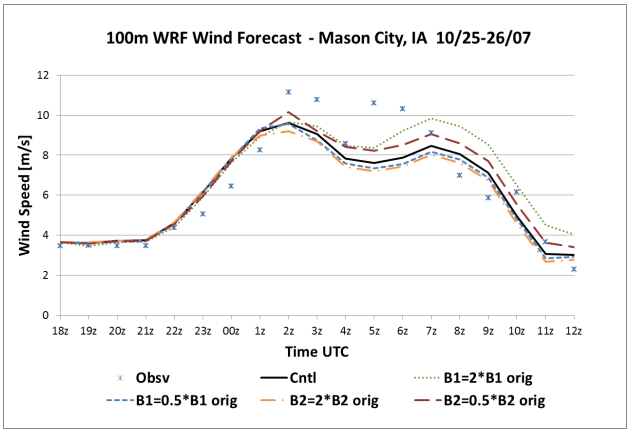

Figure 3: Time series of 100m wind forecasts for WRF simulations with varying values for $B1$ and $B2$ closure constants.

Fig. 3 shows wind forecast sensitivities to variations in $B1$ and $B2$ for one of the cases. The results are very similar for the early part of the simulations, during which time the mixed layer yet exists and the LLJ has not yet developed. There is very little creation of turbulence at 100m and thus also little dissipation of turbulence. It is thus not surprising that varying either $B1$ or $B2$ is of little significance. However, after the LLJ has developed after 1 UTC, turbulence is generated at 100m as well as dissipated and thus it is anticipated that varying the closure constants could have notable impact.

Table 1: Percentage change of each WRF wind forecast with variation of $B1$ and $B2$ relative to the control run.

Case	0.5x B1orig	2.0x B1orig	0.5x B2orig	2.0x B2orig
6/13/08	0.18	9.51	3.46	-2.41
10/25/07	-2.46	12.30	5.69	-4.30
9/19/07	-0.73	0.92	0.21	-0.97
Average	-1.00	7.59	3.12	-2.56

In Eq. 14, $B1$ exists in the denominator, thus it would seem reasonable to anticipate that the dissipation of TKE would be decreased as $B1$ is increased allowing for higher amounts of TKE to remain. The effect as seen in Table 1 when doubling the value of $B1$ is to increase the wind forecast velocities on average 7.6% across all three cases. Specifically for the case of 10/25/07, there was an overall increase of 12.30% with an instantaneous increase in velocity as high as 2 m/s later in the forecast (Fig. 3). Reducing $B1$ to half its original value did not cause as strong of response with an overall reduction in forecasted winds of only 1% across all three cases.

In consideration of forecast sensitivity to changes in $B2$, Eq. 15 dictates that an increase(decrease) in $B2$ would result in a reduction(increase) in thermodynamic dissipation. Table 1 shows the effect on the forecasted winds upon doubling $B2$ for the three cases considered. On average there is a

2.56% decrease in wind velocities as compared to the control run. On the other hand, reducing $B2$ to half of its original value results in a slightly higher absolute change in wind velocities with wind velocities increasing on average 3.12% over the control run. It is interesting to note the greatest forecast sensitivity was registered with an increase in $B1$ as compared to a reduction of this same closure constant or as compared to equal variations in $B2$.

4.2 Formulation of closure constants

Mesoscale wind forecasts were created using WRF for three wind ramp cases near Mason City, IA. Example results for one of these cases that occurred 09/15-16/08 are given in Fig. 4, which shows a time series of forecasted horizontal velocities at 50m, 100m, 150m and 200m heights. The other two LLJ cases for which mesoscale forecasts were generated (not shown) occurred also near Mason City on 9/19/07 and 6/14/08. Vertical profiles of horizontal wind and potential temperature were extracted from the 3D, 3.33-km resolution forecast domain for each case, above a surface point nearest the tall tower data at Mason City and at a time after the development of the LLJ when the solution was quasi-steady state. These profiles were used to initialize idealized LES simulations with a horizontally-homogeneous base state as described in the methodology section. A 2-hour forecast is generated, for which a time step of 1/30th of a second was required to maintain a numerically stable solution. It was found per several preliminary simulations that 2 hours were sufficient to obtain a steady-state solution as demonstrated by a near-constant vertically integrated TKE.

Variables from the LES runs were output every minute to allow for the calculation of Reynolds-averaged velocities for a given vertical height (based on a 10-minute temporal average and 2D spatial average over the horizontal domain). The Reynolds-averaged vertical profile of wind velocities after 2 hours are given in Fig. 5 and corresponding profiles of TKE in Fig. 6. TKE values were calculated using velocity variances from the Reynolds-averaged velocity at a given height along with the subgrid TKE as generated per the 1.5 TKE scheme of the LES model.

Fig. 6 shows higher TKE values are associated with cases with higher overall velocities and vertical wind shear (Fig. 5). The highest TKE values are also identified at the level just below the LLJ wind maximum, where vertical shear is yet significant and at a level where winds are close to maximum strength.

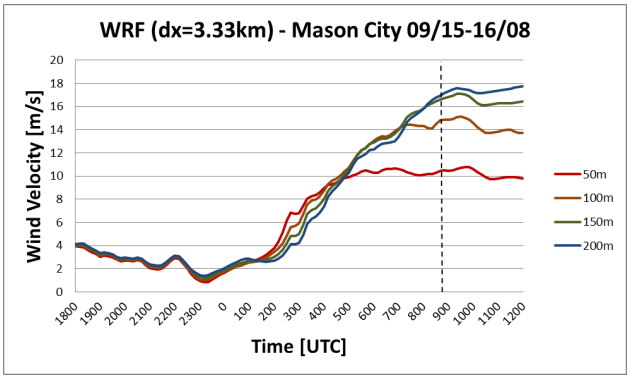

Figure 4: Mesoscale wind forecast of a wind ramp event near Mason City, IA on 09/15-16/08. Results are shown at vertical levels 50, 100, 150, and 200 meters. The vertical line indicates time at which vertical profile is extracted to initiate the LES simulation.

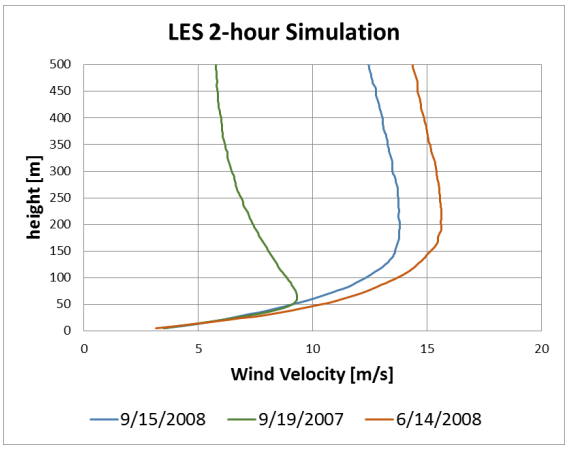

Figure 5: Vertical profiles of horizontal wind [m/s] after a 2-hour LES simulation. The values are averaged spatially over a given height level and temporally over the last 10 minutes of the simulation. Only the levels below 500m are shown.

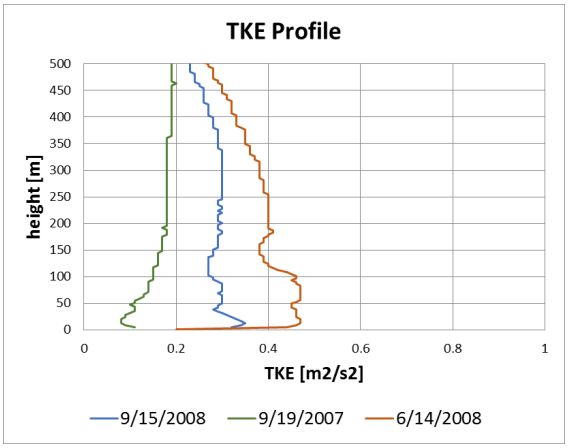

Figure 6: Vertical profiles of TKE [m^2/s^2] associated with the wind profiles as given in Fig. 5

Using the explicitly-resolved turbulence data from the LES run, various turbulence variables, such as momentum and heat fluxes, can be calculated explicitly, and most importantly, values for the closure constants can be identified. The constants $B1$ and $B2$ are calculated according to the Level 2 equations of the second-order turbulent energy model as presented in N01, specifically Eqs. 16 and 17 respectively.

$$B1 = \frac{q^3}{L}[-\overline{uw}\frac{\partial U}{\partial z} + \frac{g}{\Theta_o}\overline{w\theta}]^{-1} \tag{16}$$

$$B2 = -\frac{q\overline{\theta^2}}{L[\overline{w\theta}\frac{\partial \Theta}{\partial z}]} \tag{17}$$

The Reynold's averaged variables in eqs. 16 and 17, such as q, $\overline{uw}$, $\overline{\theta^2}$ and $\overline{w\theta}$ can be derived explicitly from the LES data.

Fig. 7 shows calculated $B1$ values based on the LES data for the 3 cases. The vertical axis represents height normalized by the level of the LLJ wind maximum, H. It is clear that $B1$ is not a constant value at all heights. This is especially true in the surface layer, the region below 20% of the height of the LLJ, for which $B1$ decreases with height, and then just below the wind maximum where $B1$ increases significantly and then switches to a negative value at a level 66% of the LLJ height. (Reasons for this trend and ramifications of a negative closure constants are discussed below).

It is interesting to note, however, that for the cases in 2008 for which there exists some vertical separation between the effect of the LLJ above the surface layer, $B1$ is semi-constant over this mid-region with an average value of 35. This suggests that a constant value for $B1$ may be appropriate within the center of a SBL, although the value of $B1 = 24$ as currently hard-coded in the MYNN scheme of WRFV3.5 would be too low for the cases considered here.

To get a better understanding of the reason for the trends in $B1$ especially in the region of the LLJ, it is worthwhile to investigate the individual terms in Eq. 16. The first term on the RHS is a shear term and the second a buoyancy term. Calculated values for these terms are plotted with height in Fig. 8. It can be seen that the shear term dominates at lower levels but its value generally reduces with height while the buoyancy term

increases its negative magnitude slightly with height. In the middle region below the LLJ, both terms seem to balance such that $B1$ maintains a near constant value with height. In the region of the LLJ, however, the shear term is reduced while the buoyancy term remains of the same (negative) magnitude. The result is that both terms nearly cancel and the denominator in Eq. 16 tends toward infinity. At slightly higher levels above the wind maximum, the negative buoyancy term dominates and thus $B1$ becomes negative.

A negative value for $B1$ would mean that a dissipation term is *generating* energy, which makes no physical sense. This result suggests that in the region of the LLJ and above, that a physical effect has been neglected, which would otherwise have bearing on the solution of $B1$. That is, using the Level 2.0 equation to determine $B1$ (as done here as well as in the study of N01) is an oversimplification and would require the use of higher-order equations for which such effects as vertical momentum fluxes and time-tendency of heat fluxes are not neglected. Such effort is part of on-going research.

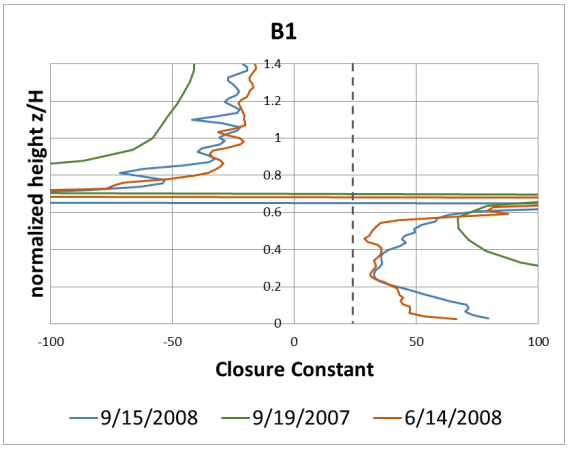

Figure 7: Calculation of the B1 closure constant based on explicitly resolved turbulence variables from the LES model for the 3 cases.

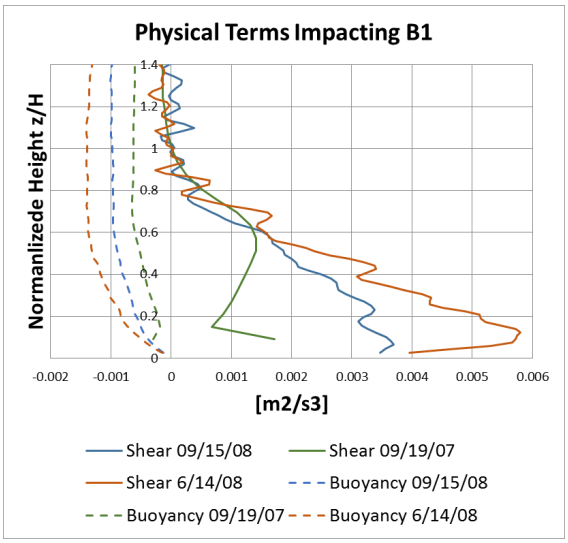

Figure 8: Specific terms in calculating $B1$ based on Eq. 16 .

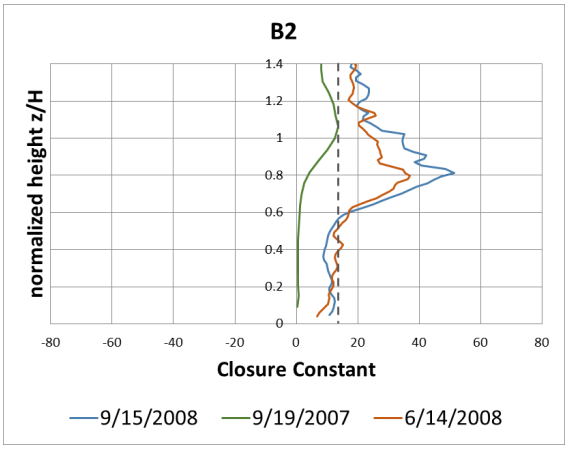

Figure 9: Values for the B2 closure constant calculated by vertical height.

The $B2$ closure constant was calculated for the three LLJ cases in this study with the same LES-generated data as used in calcuating $B1$, although based on Eq. 17. The results are shown in Fig. 9. The turbulent covariant values are spatially averaged horizontally across the domain and temporally over 10 minutes based on the LES simulation after the first two hour forecast window.

Fig. 9 shows a near constant value for $B2$ of approximately 12 to 15 for the two cases in

2008 in the region below the LLJ. Except for the case in 2007 with a LLJ at a relatively low height, these results show that setting $B2$ to a single value may be appropriate, although only within the SBL below the wind maximum. The values of $B2$ for the two 2008 cases are very close to the constant value of $B2 = 15$ as prescribed by N01 and currently set in the MYNN scheme of WRF version 3.5.

5 Summary and Future Work

The closure constants $B1$ and $B2$, which are associated with the dispersion term of the MYNN BL scheme, have been re-evaluated in context of several LLJ cases existing within a SBL. It was found that mesoscale wind forecasts show notable sensitivity to significant variations in these closure constants thus indicating that wind forecast improvement could be effected by carefully tuning these constants for the SBL. Based on fine-scale simulations of LLJ events, it was found that appopriate values for $B1$ and $B2$ may be set as constant, but only over limited regions of the SBL below the LLJ. For the cases considered in this study, results suggest a value of $B1 = 35$, which is higher than what is currently hard-coded in the MYNN scheme, $B1 = 24$. Calculated values of $B2$ for these same cases, however, propose a value of 15, which is congruent with what exists in the MYNN scheme.

These results are highly preliminary given the limited number of cases considered in this study. Future work will involve the analysis of a suite of 10-15 LLJ cases, which would help to substantiate proposed adjustments to closure constant values for the SBL.

6 Acknowledgments

The work reported herein was supported by the US National Science Foundation (NSF) through its Integrated Graduate Education and Research Traineeship (IGERT) Program, award 1069283. 162. Partial support was provided by the NSF also under the State of Iowa EPSCoR Grant 1101284. The tall tower meteorological observations were provided through the Tall Tower Wind Measurement Project that was conducted by AWS Truepower and funded by the Iowa Energy Center and the US Dept. of Energy.

References

Benjamin, S., J. Olson, E. James, C. Alexander, J. M. Brown, S. Weygandt, T. Smirnova, and J. Wilczak, 2013: Advances in model forecast skill from 2012 - 2013 assimilation and modeling enhancements to NOAA hourly updated models. *UVIG Workshop on Forecasting Applications*, Salt Lake City, UT.

Bradford, K. T., R. L. Carpenter, and B. L. Shaw, 2010: Forecasting Southern Plains wind ramp events using the WRF model at 3-km. *Ninth Annual Student Conference*, Amer. Metr. Soc., Atlanta, GA, 1–10.

Deppe, A. J., W. A. Gallus, and E. S. Takle, 2013: A WRF ensemble for improved wind speed forecasts at turbine height. *Wea. Forecasting*, **28 (1)**, 212–228.

Dudhia, J., 1989: Numerical study of convection observed during the winter monsoon experiment using a mesoscale two-dimensional model. *J. Atmos. Sci.*, **46**, 3077–3107.

F. Chen, J. D., 2001: Coupling an advanced land surface-hydrology model with

the Penn State-NCAR MM5 modeling system, part I: Model implementation and sensitivity. *Mon. Wea. Rev.*, **129**, 569–585.

Fernando, H. J. S. and J. C. Weil, 2010: Whither the Stable Boundary Layer? A Shift in the Research Agenda. *Bull. Amer. Meteor. Soc.*, **91 (11)**, 1475–1484.

Freedman, J., M. Markus, and R. Penc, 2008: Analysis of West Texas wind plant ramp-up and ramp-down events. Tech. rep., AWS Truepower, LLC, 251–278 pp.

Greaves, B., J. Collins, J. Parkes, A. Tindal, G. Hassan, S. Vincent, and S. Lane, 2009: Temporal forecast uncertainty for ramp events. *Wind Engineering*, **33 (4)**, 309–320.

Grisogono, B., 2010: Generalizing 'z-less' mixing length for stable boundary layers. *Q. J. R. Meteorol. Soc.*, **136 (646)**, 213–221.

Hong, S. Y., J. Dudhia, and S. H. Chen, 2004: A revised approach to ice microphysical processes for the bulk parameterization of clouds and precipitation. *Mon. Wea. Rev.*, **132**, 103–120.

Hu, X.-M., P. Klein, and M. Xue, 2013: Evaluation of the updated YSU planetary boundary layer scheme within WRF for wind resource and air quality assessments. *J. of Geophys. Res. Atmos.*, **118**, 10,490–10,505.

Kain, J. S., 2004: The Kain-Fritsch convective parameterization: An update. *J. Appl. Meteor.*, **43**, 170–181.

Mellor, G. and T. Yamada, 1974: Hierarchy of turbulence closure models for planetary boundary layers. *J. Atmos. Sci.*, **31**, 1791–1806.

Mellor, G. L., 1973: Analytic prediction of the properties of stratified planetary surface layers. *J. Atmos. Sci.*, **30**, 1061–1069.

Mellor, G. L. and T. Yamada, 1982: Development of a turbulence closure model for geophysical fluid problems. *Rev. Geophys.*, **20 (4)**, 851–875.

Mlawer, E. J., S. J. Taubman, P. D. Brown, M. J. Iacono, and S. A. Clough, 1997: Radiative transfer for inhomogeneous atmospheres: RRTM, a validated correlated-k model for the longwave. *J. Geophys. Res.*, **102**, 16,663–16,682.

Nakanishi, M., 2001: Improvement of the Mellor-Yamada turbulence closure model based on large-eddy simulation data. *Boundary-Layer Meteorol.*, **99 (3)**, 349–378.

Nakanishi, M. and H. Niino, 2004: An improved Mellor-Yamada level-3 model with condensation physics: its design and verification. *Boundary-Layer Meteorol.*, **112 (1)**, 1–31.

Navid, N., G. Rosenwald, and D. Chatterjee, 2011: Ramp Capability for Load Following in the MISO Markets. Tech. Rep. 1, MISO Market Development and Analysis, 1–49 pp.

Olson, J. and J. M. Brown, 2011: Modifications in the MYNN PBL/surface scheme to improve the AK coastal barrier jet and overall performance in the rapid refresh. *Proc., Alaska Weather Symp 2011*, Fairbanks, Alaska, Amer. Meteor. Soc.

Olson, J. and J. M. Brown, 2012: Modifications in the MYNN PBL and surface layer scheme for WRF-ARW. *Pro., WRF User's Workshop 2012*, Boulder, CO.

S. Schreck, W. S., J. Lundquist, 2008: U.S. dept. of energy workshop report: Research

needs for wind resource characterization. Tech. rep., National Renewable Energy Laboratory.

Storm, B. and S. Basu, 2010: The WRF model forecast-derived low-level wind shear climatology over the United States Great Plains. *Energies*, **3 (2)**, 258–276.

Yamaguchi, T. and G. Feingold, 2012: Large-eddy simulation of cloudy boundary layer with the Advanced Research WRF model. *Tech. Note, J. Adv. Model. Earth Syst.*, **4 (3)**.